PHYSICAL REVIEW B
CONDENSED MATTER

THIRD SERIES, VOLUME 41, NUMBER 15 15 MAY 1990-II

Structural properties of ordered high-melting-temperature intermetallic alloys from first-principles total-energy calculations

M. J. Mehl, J. E. Osburn, D. A. Papaconstantopoulos, and B. M. Klein
Complex Systems Theory Branch, Condensed Matter and Radiation Science Division, Naval Research Laboratory, Washington, D.C. 20375-5000
(Received 13 December 1989)

Intermetallic compounds which are ductile at high temperatures are of great technological interest; however, purely experimental searches for improved intermetallic materials are time consuming and expensive. Theoretical studies can shorten the experimental search by focusing on compounds with the desired properties. While current *ab initio* density-functional calculations cannot adequately determine material properties at high temperature, it is possible to compute the static-lattice equation of state and elastic moduli of ordered binary compounds. Known correlations between equilibrium properties and high-temperature properties such as the melting temperature can then be used to point the way for experiments. We demonstrate the power of this approach by applying the linear augmented-plane-wave method to the calculation of the equation of state and all of the zero-pressure elastic moduli for SbY in the $B1$ (NaCl) phase, CoAl and RuZr in the $B2$ (CsCl) phase, and NbIr in the $L1_0$ (Au-Cu I) phase. The calculated equilibrium lattice constants are all within 2% of the experimentally determined values. The only experimentally known elastic moduli in these systems are the bulk and shear moduli for polycrystalline SbY, CoAl, and NbIr. The predicted bulk moduli are with 7% of experiment. Theory enables us to place limits on the experimental polycrystalline shear modulus. The experimental shear moduli of SbY and CoAl are within our theoretical bounds, but the experimental shear modulus of NbIr is 35% smaller than our lower bound. We stress that in the case of CoAl our calculations provided a prediction for the bulk and shear moduli that were subsequently confirmed by the experiments of Fleischer. We also discuss the band structures and electronic density of states for these materials.

I. INTRODUCTION

New technological applications demand the increased use of metals which are strong, stiff, and ductile at high temperatures. Ideally, these metals would also be light in weight. Stable materials which have the desired properties are not the single crystals theorists favor. Intermetallic alloys are complex structures, with defects, impurities, and grain boundaries helping to stabilize the material and determine its physical properties. At the present time, theory is unable to deal with real systems of this type. One role of computational physics is to help determine materials worthy of experimental attention, and to indicate possible candidates for substitutional alloying.

Our approach is to perform calculations of the electronic structure of various ordered intermetallic alloys and from them determine the equation of state and the elastic moduli. Using known empirical correlations, these properties may then be related to other interesting physical properties such as the melting temperature[1] and the ductility. The electronic-structure calculations are performed using the linear augmented-plane-wave (LAPW) method. No shape approximations are made to the potential. This method is very accurate and represents the state of the art in band-structure calculations. We applied the LAPW method to obtain the self-consistent electronic structure, equation of state, equilibrium lattice constants, and elastic moduli for several ordered binary intermetallic compounds. We present our work on the SbY ($B1$ structure), CoAl ($B2$ structure), RuZr ($B2$ structure), and NbIr ($L1_0$ structure) systems. In addition, we use the correlations discovered by Fine *et al.*[1] to predict the melting temperature. We emphasize that all of the structural parameters and elastic-moduli calculations are of the first-principles type; that is, the crystal structure and the elemental atomic numbers are the only inputs.

Extension of this process to more complicated materials is difficult. The LAPW method is computer-time intensive, and for compounds with more than ten atoms per unit cell its use becomes prohibitively expensive given the capabilities of present-day computers. We may, however,

Work of the U. S. Government
Not subject to U. S. copyright

use the information obtained in these simple systems as input for modeling larger systems. For example, the equations of state and elastic moduli determined here can be used as input to determine the parameters needed to do embedded-atom calculations.[2] This is particularly important in systems such as RuZr, where no single-crystal measurements of elastic constants have been performed.

The paper is organized as follows. In Sec. II we describe the details of the LAPW calculations and the determination of the equilibrium lattice constants. In Sec. III we present the method of evaluation of the elastic constants. In Sec. IV we discuss our predictions for the mechanical behavior of the intermetallics SbY, CoAl, RuZr, and NbIr, including comparison with experiment. The electronic structure of these intermetallics is examined in Sec. V. In Sec. VI we summarize our results.

II. TOTAL-ENERGY CALCULATIONS: EQUILIBRIUM LATTICE DETERMINATION

The equilibrium structural parameters were determined using total energies obtained by the self-consistent full-potential linear augmented-plane-wave (LAPW) method of Andersen,[3] using the program of Wei and Krakauer.[4] This procedure has been previously tested on the intermetallic TiAl,[5] where the computed lattice constants were found to be in good agreement with experiment. Following the usual procedure, we divided the electronic states of the system into core, semicore, and valence bands. The core eigenstates were calculated using a fully relativistic spherical integration routine, while the semicore and valence states were found by diagonalizing the Hamiltonian using the LAPW basis functions and the semirelativistic (averaged spin-orbit interaction) approximation.[6] To allow more variational freedom in each band, the valence and semicore states were diagonalized separately. The nominal atomic states in the valence and semicore windows are listed in Table I. Brillouin-zone integrals were approximated using the special-**k**-points method of Monkhorst and Pack,[7] with slight modifications as outlined below. Table I lists the number of **k** points used in each window for the equation-of-state calculations. We found that these selections of **k** points provided satisfactory convergence of the equation of state. The Kohn-Sham single-particle potentials were found with use of the Hedin-Lundqvist parametrization[8] of the local-density approximation (LDA) to Hohenberg-Kohn density-functional theory.[9] Iteration was stopped when the total energy changed by less than 0.01 mRy between iterations.

We began the determination of the equilibrium properties of the intermetallics by calculating the total energy as a function of the unit-cell volume for the cubic materials and as a function of the volume and c/a for the tetragonal $L1_0$ structure. The number of points used in each case may be found in Table I. The equilibrium structures were determined by making a least-squares fit of the total energy versus the lattice parameters to a model equation of state. For the cubic intermetallics SbY, CoAl, and RuZr we used the form proposed by Birch:[10]

$$E(V)=\sum_{n=0}^{N} a_n V^{-2n/3} , \tag{1}$$

where V is the volume of the unit cell. The minimum-energy volume was found by minimizing (1), and the equilibrium bulk modulus was determined from the definition

$$B(V)=VE''(V) . \tag{2}$$

For the calculations in this paper, we chose $N=3$. Fitting to higher powers of $V^{-2/3}$ (where possible) did not significantly change the results.

The tetragonal $L1_0$ phase of NbIr (see Fig. 1) has two lattice parameters, a and c, with primitive vectors

$$\begin{aligned} \mathbf{a}_1&=(\tfrac{1}{2}a,-\tfrac{1}{2}a,0) ,\\ \mathbf{a}_2&=(\tfrac{1}{2}a,\tfrac{1}{2}a,0) ,\\ \mathbf{a}_3&=(0,0,c) , \end{aligned} \tag{3}$$

and basis vectors

$$\begin{aligned} \mathbf{b}_1&=(0,0,0)\\ \mathbf{b}_2&=\tfrac{1}{2}(\mathbf{a}_1+\mathbf{a}_2+\mathbf{a}_3)=(\tfrac{1}{2}a,0,\tfrac{1}{2}c) . \end{aligned} \tag{4}$$

TABLE I. Numerical parameters used for LAPW equation of calculations.

	Compound			
	SbY	CoAl	RuZr	NbIr
Structure	$B1$	$B2$	$B2$	$L1_0$
Symmetry	cubic	cubic	cubic	tetragonal
Number of lattice constants computed	5	4	5	35
Number of windows	2	1	2	2
Number of special **k** points [valence- (semicore)]	28 (2)	10	20 (10)	30 (6)
Valence states	Sb $5p$ Y $4d,5s$	Co $3d,4s$ Al $3s,3p$	Ru $4d,5s$ Zr $4d,5s$	Nb $4d,5s$ Ir $5d,6s$
Semicore states	Sb $4d,5s$ Y $4s,4p$		Ru $4s,4p$ Zr $4s,4p$	Nb $4p$

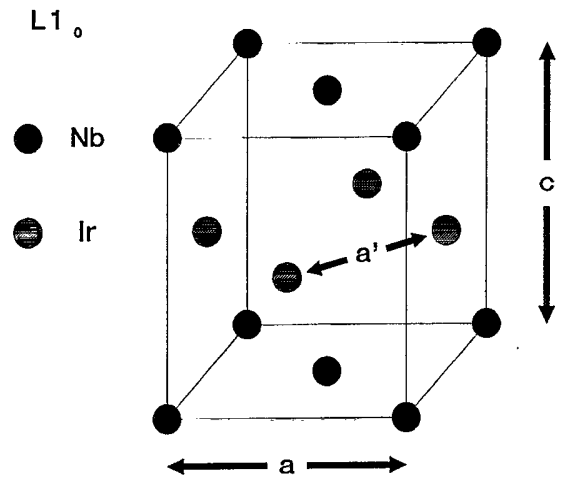

FIG. 1. The $L1_0$ structure of NbIr. The niobium atoms are represented by solid circles, the iridium atoms by shaded circles. The distances a and c describe the lattice in terms of the primitive vectors (3), while the distances a' and c describe the lattice in terms of the primitive vectors (16).

Obviously, a fit to the simple formula (1) at fixed c/a is not adequate. To overcome this difficulty, we did LAPW calculations at five different c/a ratios for each volume. At each volume we fit the energy to a third-order polynomial in c/a. Since the equilibrium c/a ratio for NbIr is near unity, these polynomials always had local minima near $c/a=1$. The precise value of this local minimum was denoted the c/a ratio for this volume, and the corresponding energy was used to determine the energy-versus-volume equation of state. This was then fit to the Birch form (1), and from there the equilibrium volume and bulk modulus were found. The remaining parameter c/a was determined by fitting to the Birch-like form:

$$(c/a)(V)=\sum_{n=0}^{N} z_n V^{-2n/3} , \tag{5}$$

where $(c/a)(V)$ is the value of c/a which minimizes the energy at the fixed volume V.

III. TOTAL-ENERGY CALCULATIONS: ELASTIC-MODULI COMPUTATIONS

The LAPW method allows total-energy calculations to be done for arbitrary crystal structures. We can therefore apply small strains to the equilibrium lattice, determine the resulting change in the total energy, and from this information deduce the elastic moduli. The calculation of the moduli allows us to garner information about nonequilibrium properties from our simple initial system. First of all, of course, the elastic moduli give direct information about the stiffness of the crystal, and ΔE's departure from quadratic behavior can give information about the ductility. In addition, using the correlations discovered by Fine *et al.*,[1] we can use the equilibrium elastic moduli to make a rough estimate of the melting temperature. Our determination of the equilibrium structural parameters and elastic moduli can also be used as a database to determine parameters for model systems such as the embedded-atom method.[2] Methods such as this have been used to consider defects and cracks in metals. Thus our calculations can be extended in ways far beyond the direct capabilities of the method.

We already have sufficient data to determine the bulk modulus as a function of volume, Eq. (2). We calculate $B(V)$ by doubly differentiating the Birch fit (1), remembering that, for the tetragonal NbIr system, $E(V)$ must be evaluated at the c/a ratio which minimizes the energy.

For later use, we now present the relationship between the bulk modulus and the elastic moduli C_{ij}. For the systems considered here,[11]

$$B=\tfrac{1}{3}(C_{11}+2C_{12}) \quad \text{(cubic lattice)} \tag{6}$$

and

$$B=\frac{(C_{11}+C_{12})C_{33}-2C_{13}^2}{C_{11}+C_{12}+2C_{33}-4C_{13}} \quad \text{(tetragonal lattice)} . \tag{7}$$

The remaining elastic moduli require additional calculations beyond the simple equation of state. We determine linear combinations of the C_{ij} by straining the crystal and relating the change in energy as a function of the strain to the elastic moduli.[12,13] Following the notation of Ref. 12, we distort the lattice by applying a small strain which transforms the lattice vectors a according to the rule

$$\overleftrightarrow{\mathbf{a}}'=(\overleftrightarrow{\mathbf{I}}+\overleftrightarrow{\epsilon})\cdot\overleftrightarrow{\mathbf{a}} , \tag{8}$$

where $\overleftrightarrow{\mathbf{a}}'$ ($\overleftrightarrow{\mathbf{a}}$) is a matrix containing the components of the new (old) lattice vectors, $\overleftrightarrow{\mathbf{I}}$ is the 3×3 identity matrix, and $\overleftrightarrow{\epsilon}$ is a matrix containing the strain components. There are many distortions which can be used to determine the elastic moduli. Ideally, we would choose the shears which minimize the amount of computer time and memory needed to do the calculations. Thus we will tend to choose highly symmetric strained lattices, since this limits the number of special **k** points needed to obtain accurate total energies.

A cubic crystal has three independent elastic moduli. We may consider them to be the bulk modulus (6), $C_{11}-C_{12}$, and C_{44}. For the calculation of the tetragonal shear modulus $C_{11}-C_{12}$, we considered two possible strains, a volume-conserving tetragonal strain,

$$\overleftrightarrow{\epsilon}=\begin{bmatrix} e_1 & 0 & 0 \\ 0 & e_1 & 0 \\ 0 & 0 & (1+e_1)^{-2}-1 \end{bmatrix} , \tag{9}$$

with energy change

$$\Delta E=3V(C_{11}-C_{12})e_1^2+O(e_1^3) , \tag{10}$$

where V is the volume of the unit cell, and an orthorhombic shear,

$$\overleftrightarrow{\epsilon}=\begin{bmatrix} e_1 & 0 & 0 \\ 0 & -e_1 & 0 \\ 0 & 0 & e_1^2/(1-e_1^2) \end{bmatrix}, \tag{11}$$

with energy change

$$\Delta E(e_1)=\Delta E(-e_1)=V(C_{11}-C_{12})e_1^2+O(e_1^4)\ . \tag{12}$$

The higher-symmetry tetragonal shear (9) allows the use of fewer special **k** points than the orthorhombic shear (11) in the self-consistent energy calculations. This is more than offset by the fact that the energy change (12) is an even function of the strain e_1, halving the number of total-energy calculations which must be done to obtain enough information to determine the elastic modulus. We determined $C_{11}-C_{12}$ for SbY and RuZr by use of the strain (11), while $C_{11}-C_{12}$ for CoAl was found using (9).

The remaining independent modulus, C_{44}, was found by shearing the crystal with the monoclinic strain,

$$\overleftrightarrow{\epsilon}=\begin{bmatrix} 0 & \frac{1}{2}e_6 & 0 \\ \frac{1}{2}e_6 & 0 & 0 \\ 0 & 0 & e_6^2/(4-e_6^2) \end{bmatrix}. \tag{13}$$

The energy associated with this strain is

$$\Delta E(e_6)=\Delta E(-e_6)=\tfrac{1}{2}VC_{44}e_6^2+O(e_6^4)\ . \tag{14}$$

Like (12), the energy associated with the shear (13) is even in the strain parameter.

The tetragonal $L1_0$ structure has six elastic moduli. The moduli $C_{11}+C_{12}$, C_{13}, and C_{33} could, in principle, be determined from the data already taken in finding the equation of state.[5] One example of this is the calculation of the bulk modulus (7) using Eq. (2). Another example is the modulus

$$K_{\text{fix}}=\tfrac{1}{9}[2(C_{11}+C_{12})+C_{33}+4C_{13}]\ , \tag{15}$$

which can be determined by considering the energy as a function of volume at fixed c/a, and is, in fact, an upper bound on the bulk modulus.[14] Unfortunately, as we shall see below, the difference $K_{\text{fix}}(V)-B(V)$ is smaller than the estimated error in our calculations, so that we cannot use (7) and (15) to separate the contributions of the individual C_{ij}. We will therefore determine all six elastic moduli by calculating the change in total energy due to a lattice strain (8). The specific strains used to determine the specific moduli are listed in Table II. Whenever possible, the strains are chosen so that the change in energy is even in the strain.

The elastic moduli listed in Table II are calculated relative to the crystal structure given by (3) and (4). This structure may be considered an fcc Nb lattice with every other (001) plane of Nb atoms replaced by Ir atoms. Alternatively, we can consider the $L1_0$ structure a body-centered-tetragonal lattice, with alternating planes of Nb replaced by Ir. In this case the lattice can be represented by the primitive vectors

$$\begin{aligned} \mathbf{a}_1&=(a',0,0)\ , \\ \mathbf{a}_2&=(0,a',0)\ , \\ \mathbf{a}_3&=(0,0,c)\ , \end{aligned} \tag{16}$$

and the basis vectors

$$\begin{aligned} \mathbf{b}_1&=(0,0,0)\ , \\ \mathbf{b}_2&=\tfrac{1}{2}(\mathbf{a}_1+\mathbf{a}_2+\mathbf{a}_3)=(\tfrac{1}{2}a',\tfrac{1}{2}a',\tfrac{1}{2}c)\ , \end{aligned} \tag{17}$$

where $a'=a/\sqrt{2}$, rather than by (3) and (4). This lattice can be obtained from (3) and (4) by making a 45° rotation about the z axis. Since the C_{ij} are actually components of a fourth-order tensor, the components in the old (unprimed) and new (primed) frames are related by

$$\begin{aligned} &C'_{11}+C'_{12}=C_{11}+C_{12},\quad C'_{11}-C'_{12}=2C_{66}\ , \\ &C'_{66}=\tfrac{1}{2}(C_{11}-C_{12}),\quad C'_{13}=C_{13}\ , \\ &C'_{33}=C_{33},\quad C'_{44}=C_{44}\ . \end{aligned} \tag{18}$$

This choice of axis is standard for a tetragonal structure.

TABLE II. Strains and elastic moduli for the tetragonal $L1_0$ phase of NbIr.

Strain	Parameters (unlisted $e_i=0$)	$\Delta E/V$ [to $O(e^2)$]
1	$e_2=e_1$	$(C_{11}+C_{12})e_1^2$
2	$e_2=e_1\quad e_3=(1+e_1)^{-2}-1$	$(C_{11}+C_{12}+2C_{33}-4C_{13})e_1^2$
3	e_3	$\frac{1}{2}C_{33}e_3^2$
4	$e_1=[(1+x)/(1-x)]^{1/2}-1,\quad e_2=-e_1/(1+e_1)$	$(C_{11}-C_{12})x^2$
5	$e_5=e_4,\quad e_3=e_4^2/4$	$C_{44}e_4^2$
6	$e_6,\quad e_1=e_2=(1+e_6^2/4)^{1/2}-1$	$\frac{1}{2}C_{66}e_6^2$

Strain matrix:

$$\overleftrightarrow{\epsilon}=\begin{bmatrix} e_1 & \frac{1}{2}e_6 & \frac{1}{2}e_5 \\ \frac{1}{2}e_6 & e_2 & \frac{1}{2}e_4 \\ \frac{1}{2}e_5 & \frac{1}{2}e_4 & e_3 \end{bmatrix}$$

Doing Brillouin-zone integrations in strained lattices requires special attention to the choice of **k** points. Our general scheme for generating special **k** points is taken from the work of Monkhorst and Pack.[7] Problems can arise with this method, however, when the primitive vectors which are used to generate the **k** points are not orthogonal. In the limit of zero strain $\overleftrightarrow{\epsilon}$, we can group the special **k** points into "stars" which are equivalent under the full set of symmetry operations for the lattice. If the star is not complete (i.e., there are other **k** points, not in the original list, which are equivalent under the full set of symmetry operations but not under the reduced set of the strained lattice), then the **k**-point-integration mesh does not recognize anything special about the zero-strain lattice. As a result, the computed stress need not vanish at zero strain, and the values deduced for the elastic moduli will be incorrect. The solution is to generate a set of **k** points for the high-symmetry lattice, enlarge the set to find all **k** points which are identical with any **k** point in the original set under any transformation in the high-symmetry space group, and then group the **k** points which are identical under the lower symmetry of the strained lattice. The resulting **k** points have the proper symmetry at zero strain, and stress is guaranteed to vanish at zero strain. When the primitive vectors are orthogonal, the stars are complete, so in this paper only the fcc lattice of SbY requires this treatment.

After choosing the strain matrix $\overleftrightarrow{\epsilon}$, determining the appropriate space-group operations, and selecting a special-k-point mesh, we are finally ready to calculate elastic moduli. As an example, we outline the process used to determine $C_{11}-C_{12}$ using the orthorhombic strain (11). First, we use the LAPW method to calculate $E(e_1)$ for several strains e_1, including $E(e_1=0)$, the energy at zero strain, at fixed volume. By (12), ΔE is even in e_1, so we next fit $\Delta E(e_1)$ to a polynomial in e_1^2,

$$p(e_1^2)=\sum_{m=0}^{M} c_m e_1^{2m} . \tag{19}$$

Comparing (19) to the energy expansion (12), we see that

$$C_{11}-C_{12}=c_1/V . \tag{20}$$

A rough estimate of the error can be made by noting how c_1 changes with M.

Since single crystals of these intermetallic compounds have not been produced experimentally, experimental determinations of the elastic moduli used polycrystalline samples. These measured elastic moduli are averaged values of the single-crystal C_{ij}. If we assume that the polycrystalline sample is homogenous and isotropic, we can use elasticity theory to place bounds on the possible experimental measurements of the bulk modulus and the shear modulus.[14] For the cubic lattices, the averaged bulk modulus is identical to the single-crystal bulk modulus. For the tetragonal $L1_0$ phase of NbIr, however, the isotropically averaged bulk modulus is bounded from above by the Voigt approximation.:[15]

$$B_V=\tfrac{1}{9}(2C_{11}+C_{33}+2C_{12}+4C_{13}) , \tag{21}$$

and from below by the Reuss approximation,[16] which is identical to the single-crystal bulk modulus (6).

An isotropic material has only one shear modulus, usually denoted G. In an isotropic solid,[14]

$$G=C_{44}=\tfrac{1}{2}(C_{11}-C_{12}) . \tag{22}$$

We can compare our calculated shear moduli to experiment using the other bounds discovered by Voigt and Reuss. For a cubic crystal, G is bounded from above by[15]

$$G_V=\tfrac{1}{5}(C_{11}-C_{12}+3C_{44}) , \tag{23}$$

and from below by[16]

$$G_R=5(C_{11}-C_{12})C_{44}/[4C_{44}+3(C_{11}-C_{12})] . \tag{24}$$

Analogous expressions hold for the tetragonal lattice, where the Voigt approximation (upper bound) is[15]

$$G_V=\tfrac{1}{15}(2C_{11}+C_{33}-C_{12}-2C_{13}+6C_{44}+3C_{66}) , \tag{25}$$

while the Reuss approximation (lower bound) is[16]

$$G_R=15/(8s_{11}+4s_{33}-4s_{12}-8s_{13}+6s_{44}+3s_{66}) . \tag{26}$$

The s_{ij} are the compliance constants[11]

$$\begin{aligned} &s_{11}+s_{12}=C_{33}/C, \quad s_{11}-s_{12}=1/(C_{11}-C_{12}) , \\ &s_{13}=-C_{13}/C, \quad s_{33}=(C_{11}+C_{12})/C , \\ &s_{44}=1/C_{44}, \quad s_{66}=1/C_{66} , \end{aligned} \tag{27}$$

where

$$C=C_{33}(C_{11}+C_{12})-2C_{13}^2 . \tag{28}$$

IV. EQUATION OF STATE AND ELASTIC-MODULI RESULTS

We used the LAPW method described above to calculate the equation of state and equilibrium lattice parameters of SbY in the $B1$ phase, CoAl and RuZr in the $B2$ phase, and NbIr in the tetragonal $L1_0$ phase. As summarized above, we found the equation of state by fitting the energies $E(V)$ to the Birch equation (1) with $N=3$. The Birch fit works extremely well, giving a rms error of less than 0.05 eV for each of the four crystals. As samples of our work we show the equation of state of SbY and the Birch fit to it in Fig. 2, and the energy as a function of volume at fixed c/a for NbIr in Fig. 3. As can be seen in Fig. 3, the minimum-energy c/a value is close to 0.968 for the entire range of volumes shown.

Table III presents our results for the equilibrium lattice constants of SbY, CoAl, RuZr, and NbIr. The computed lattice constants, which neglect zero-point motion and thermal expansion, are within 2% of the experimental lattice constants[17–19] for all of the crystals. This error is on the same order as found in previous LAPW calculations.[5] We conclude that the local-density-approximation (LDA) is indeed able to determine the equilibrium lattice constants of these materials to very good accuracy.

We have also calculated all of the independent elastic moduli for the four intermetallic alloys at the lattice constants listed in Table III. Although the moduli are

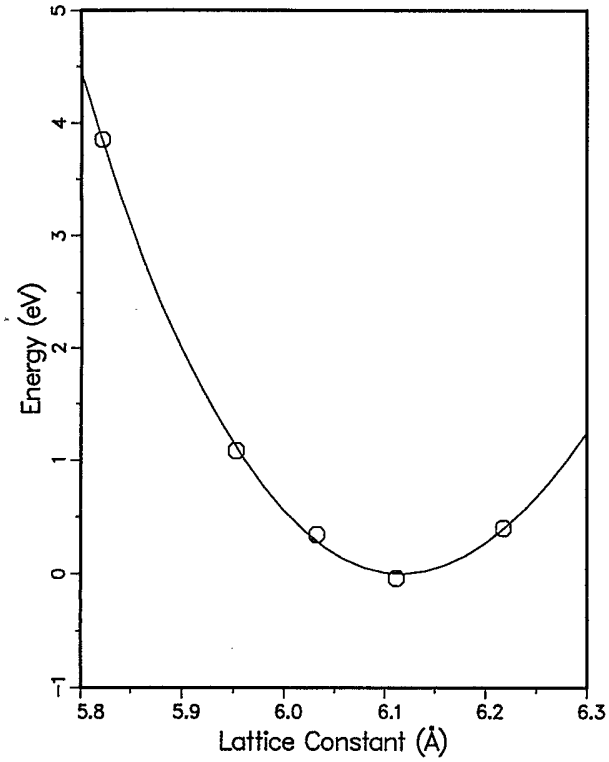

FIG. 2. The equation of state of SbY in the $B1$ (rocksalt) phase. The circles represent the calculated energies, and the solid line is a third-order Birch fit to the data. The LAPW energy has been shifted so that the minimum lattice energy is at 0 eV.

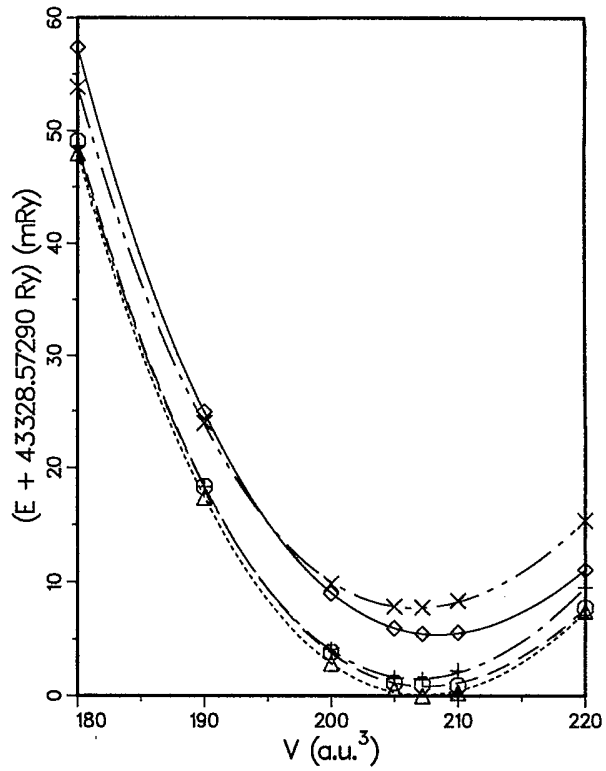

FIG. 3. Energy vs volume at fixed c/a for NbIr in the tetragonal $L1_0$ phase. The symbols represent *ab initio* data points, while the lines are third-order Birch fits [Eq. (1)] at fixed c/a. Notation: The diamonds and solid line represent $c/a=0.9$, the circles and dashed line $c/a=0.95$, the triangles and dotted line $c/a=0.968$, the pluses and dashed-dotted line $c/a=1.0$, and the x's and dashed–double-dot line $c/a=1.05$.

volume dependent, we expect the change in modulus from the LDA equilibrium volumes to the experimental volumes to be small. In Fig. 4 we plot the results of a typical calculation, using the monoclinic strain (13) to determine C_{44} for CoAl. Fits of the data to polynomials of order $M=1$, 2, 3, and 4 in e_6^2, as outlined in Sec. III, give $C_{44}=1.24$, 1.33, 1.32, and 1.26 Mbar, respectively. In light of this analysis, and allowing for numerical noise, we assign $C_{44}=1.30\pm0.05$ Mbar. The other moduli are determined in a similar manner. Table IV summarizes our results.

We may now compare our numbers to experiment. The moduli in Table IV are our predictions for perfect single crystals. We used the Voigt and Reuss bounds [Eqs. (21)–(28)] to place bounds on the polycrystalline bulk modulus B and shear modulus G. Our predictions are compared to the available experimental data[20,21] in Table V. It should be emphasized that our theoretical values for the bulk and shear moduli of CoAl were made before we obtained the experimental data. Our predictions for the bulk moduli are in excellent agreement with experiment, as are the shear moduli of SbY and CoAl. The odd point is the shear modulus of NbIr, which is approximately 15% lower than our lowest estimated bound on G. This is most likely caused by the fact that the experimental sample was 52% Nb and 48% Ir.[20]

The computed values of C_{ij} may also be used to test the correlation between elastic moduli and melting temperature discovered by Fine *et al.*[1] For cubic materials Fine *et al.* found that the data comparing melting temperatures and the equilibrium value of C_{ii} could be fitted by the straight line

$$T_m=553\text{ K}+(591\text{ K/Mbar})C_{11}\pm300\text{ K}\ , \tag{29}$$

$$T_m=354\text{ K}+(450\text{ K/Mbar})[\tfrac{1}{3}(2C_{11}+C_{33})]\pm300\text{ K}\ . \tag{30}$$

TABLE III. Equilibrium lattice constants—comparison with experiment. (RT denotes room temperature.)

	Compound			
	SbY	CoAl	RuZr	NbIr
Theory				
a (Å)	6.12	2.80	3.22	3.99
c (Å)				3.86
c/a				0.967
Expt. (RT)				
a (Å)	6.16[a]	2.86[b]	3.253[c]	4.027[d]
c (Å)				3.863[d]
c/a				0.9578[d]

[a]Reference 17, p. 807.
[b]Reference 18; Ref. 19, p. 109.
[c]Reference 19, p. 374.
[d]Reference 19, p. 296.

TABLE IV. Calculated elastic moduli.

	Compound				
	SbY	CoAl	RuZr	NbIr[a]	NbIr[b]
Lattice constant					
a (Å)	6.11	2.862	3.22	3.99	3.99
c (Å)				3.86	3.86
Bulk modulus (Mbar)	0.68±0.01	1.57±0.01	2.25±0.10	3.2±0.3	3.2±0.3
C_{11} (Mbar)	1.75±0.02	2.57±0.04	3.72±0.10	4.3±0.2	5.8±0.2
C_{12} (Mbar)	0.15±0.01	1.07±0.05	1.52±0.10	2.7±0.2	1.2±0.2
C_{13} (Mbar)				2.5±0.2	2.5±0.2
C_{33} (Mbar)				4.9±0.2	4.9±0.2
C_{44} (Mbar)	0.255±0.01	1.30±0.05	0.78±0.02	1.75±0.05	1.75±0.05
C_{66} (Mbar)				2.3±0.1	0.8±0.1

[a]Lattice parameters in Eq. (3).
[b]Lattice parameters in Eq. (16).

Another correlation[1] is that between the bulk modulus of a cubic metal and its melting temperature,

$$T_m = 607\ \text{K} + (930\ \text{K/Mbar})B \pm 500\ \text{K}\ . \tag{31}$$

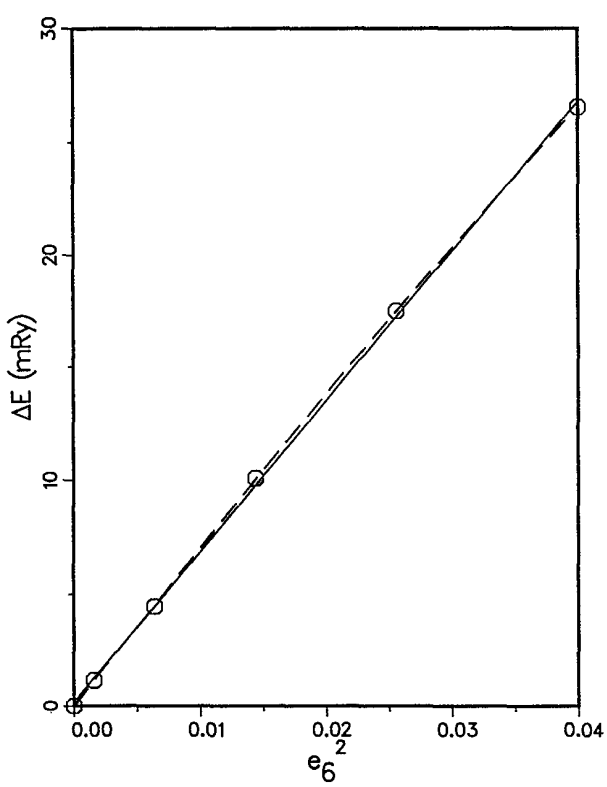

FIG. 4. The change in the total energy of CoAl under the monoclinic strain (13), used to determine C_{44}. The circles are the *ab initio* values. The solid line is a linear fit to the data, and the dashed line is a quadratic fit. The third- and fourth-order polynomial fits (not shown) are nearly identical to the quadratic fit.

The "errors" listed above represent the 68% confidence level as determined from Figs. 1, 2, and 4 of Ref. 1.

In the last section of Table V we use our calculated elastic moduli to calculate a melting temperature for each of the intermetallics. The C_{ii} used for $L1_0$ NbIr are those associated with the lattice described by the primitive vectors (16) and the basis vectors (17). The first set of theoretical calculations are based on the correlations (29) or (30), while the second set are based on (31). The "error" terms include both the uncertainties included in (29)–(31), as well as the uncertainties in our elastic-moduli calculations. Except for SbY, the difference between the predicted and experimental[22] melting temperatures is no greater in magnitude than twice the "error." Since our predicted moduli are in good agreement with the experimental data for SbY, it is clear that the failure is in the correlations (29) and (31), not in our calculation of the elastic moduli. The correlations (29)–(31) are useful in guiding experiments, but obviously do not absolutely determine the melting temperature.

V. ELECTRONIC STRUCTURE OF THE INTERMETALLIC ALLOYS

Although the main purpose of this paper is to calculate equilibrium lattice parameters and elastic constants, in this section we discuss the energy bands and densities of states. The level of accuracy required for these quantities is significantly lower than for the total-energy determinations. For this reason we use the equilibrium lattice parameters from our LAPW total-energy calculations to perform a final set of calculations for the cubic materials using the faster Slater augmented-plane-wave (APW) method in the muffin-tin (MT) approximation. In all other respects (the scalar-relativistic approximation, Hedin-Lundqvist exchange, etc.) the APW calculations were done in the same way as the LAPW calculations. The APW code has the advantage that it is symmetrized and

TABLE V. Comparison of elastic moduli with experiment.

	Compound			
	SbY	CoAl	RuZr	NbIr
Bulk modulus (Mbar)				
Expt.	0.66[a]	1.62±3%[b]		3.01[a]
Theor. upper limit	0.67±0.01	1.57±0.01	2.25±0.10	3.2±0.3
Theor. lower limit	0.67±0.01	1.57±0.01	2.25±0.10	3.2±0.2
Shear modulus (Mbar)				
Expt.	0.405[a]	1.14±3%[b]		0.993[a]
Theor. upper limit	0.460±0.01	1.08±0.04	0.91±0.03	1.55±0.2
Theor. lower limit	0.310±0.01	1.01±0.04	0.88±0.03	1.35±0.2
Melting temperature (K)				
Expt.	2580[c]	1700[c]	2100[c]	2200
Theor. [Eqs. (29) and (30)]	1590±310	2070±310	2720±360	2830±390
Theor. [Eq. (31)]	1240±510	2070±510	2650±590	

[a]Reference 20.
[b]Reference 21.
[c]Reference 22.

conveniently labels the symmetry of each state. The densities of states (DOS's) were calculated by the tetrahedron method using interpolated eigenvalues and l components of the MT charges found by a Fourier-series interpolation that accounts for the symmetry of each state.[23]

The MT approximation introduces a small error, which should be negligible for the purpose of presenting the DOS's in cubic metals. In addition, the LAPW and APW methods use slightly different basis functions, which may introduce small changes in the DOS. To check the magnitude of these effects, we calculated the eigenvalues of SbY at the high-symmetry points Γ, X, W, and L, using both the APW and LAPW methods. We shifted the potentials in both systems so that $E_F=0$. (The unshifted Fermi energy is 0.4005 Ry for the LAPW calculation and 0.3834 Ry for the APW one.) The shifted eigenenergies are compared in Table VI. The symmetry assigned to each APW state was determined by the symmetrized code. The LAPW symmetry was determined by matching the muffin-tin charge for each l component of the density of states with the corresponding APW state. One sees that the APW and LAPW programs switch the

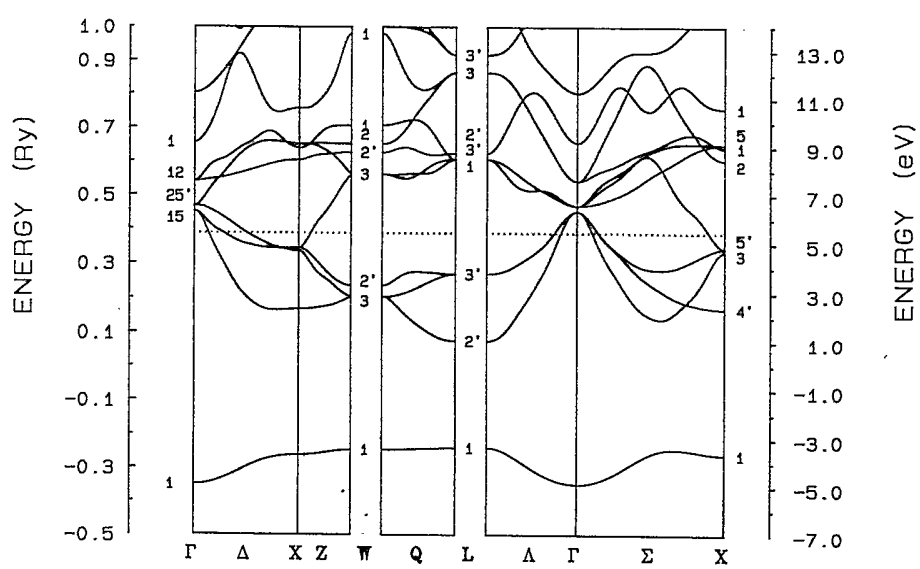

FIG. 5. The band structure along high-symmetry directions of the $B1$ phase of SbY at the lattice constant $a=6.11$ Å, calculated using the APW method. The dotted horizontal line represents the Fermi level.

TABLE VI. Comparison of APW and LAPW eigenvalues (in Ry) for SbY.

State	$E_F=0$ Ry Eigenvalues APW	LAPW	Difference
Γ_1	−0.7331	−0.7382	−0.0051
Γ_{15}	0.0694	0.0571	−0.0123
$\Gamma_{25'}$	0.0852	0.0756	−0.0096
Γ_{12}	0.1572	0.1237	−0.0335
X_1	−0.6446	−0.6531	−0.0085
$X_{4'}$	−0.2158	−0.2144	0.0014
X_3	−0.0483	−0.0380	0.0103
$X_{5'}$	−0.0393	−0.0532	−0.0139
X_2	0.2200	0.1862	−0.0338
W_1	−0.6292	−0.6377	−0.0085
W_3	−0.1801	−0.1794	0.0007
$W_{2'}$	−0.1477	−0.1687	−0.0210
W_3	0.1770	0.1700	−0.0070
L_1	−0.6240	−0.6313	−0.0073
$L_{2'}$	−0.3089	−0.3151	−0.0062
$L_{3'}$	−0.1152	−0.1363	−0.0211

order of the $X_{5'}$ and X_3 states. Otherwise, there is good agreement between the two methods, with the eigenvalues differing by no more than 0.03 Ry, and by no more than 0.02 Ry for states below E_F.

In Fig. 5 we show the energy bands of SbY in the $B1$ (NaCl) structure. The bands near the Fermi level (E_F) are predominantly a mixture of p Sb and d Y states. For example, at point Γ the state Γ_{15} has p Sb character, while the $\Gamma_{25'}$ and Γ_{12} states have d Y character. The distribution of states is more clearly seen in Fig. 6, which

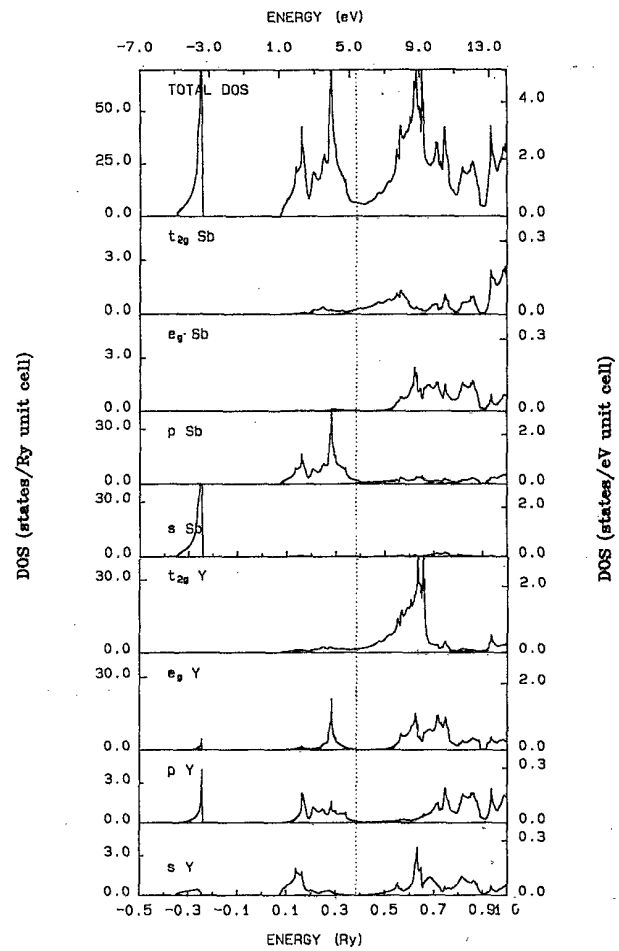

FIG. 6. The density of states of the $B1$ phase of SbY at the lattice constant $a=6.11$ Å, calculated via the APW method. The top graph shows the total density of states. The lower graphs show the partial density of states at each atom site, decomposed by the symmetry of the state. The Fermi level is represented by the dotted vertical line. Note the different scales between the d and the s,p components of the DOS.

TABLE VII. (a) Density of states at the Fermi level, and (b) l components of the DOS at E_F.

(a)

	E_F	DOS
SbY	0.383 40	6.099 84
CoAl	0.822 79	8.109 00
RuZr	0.397 08	5.873 36
NbIr	0.835 95	21.44

(b)

Crystal	Site	s	p	e_g	t_{2g}	f
SbY	Sb	0.009 98	1.843 95	0.018 19	0.241 83	0.011 71
	Y	0.021 23	0.115 09	0.216 59	1.413 72	0.066 10
CoAl	Co	0.096 35	0.500 57	5.181 81	0.936 17	0.009 81
	Al	0.014 85	0.420 95	0.006 54	0.177 73	0.005 51
RuZr	Ru	0.542 11	0.823 76	0.035 19	0.081 21	0.030 25
	Zr	0.418 10	0.550 22	0.301 44	0.487 40	0.039 73
				d		
NbIr	Nb	0.1686	0.5948	8.718		0.1527
	Ir	0.0806	0.8058	5.405		0.0648

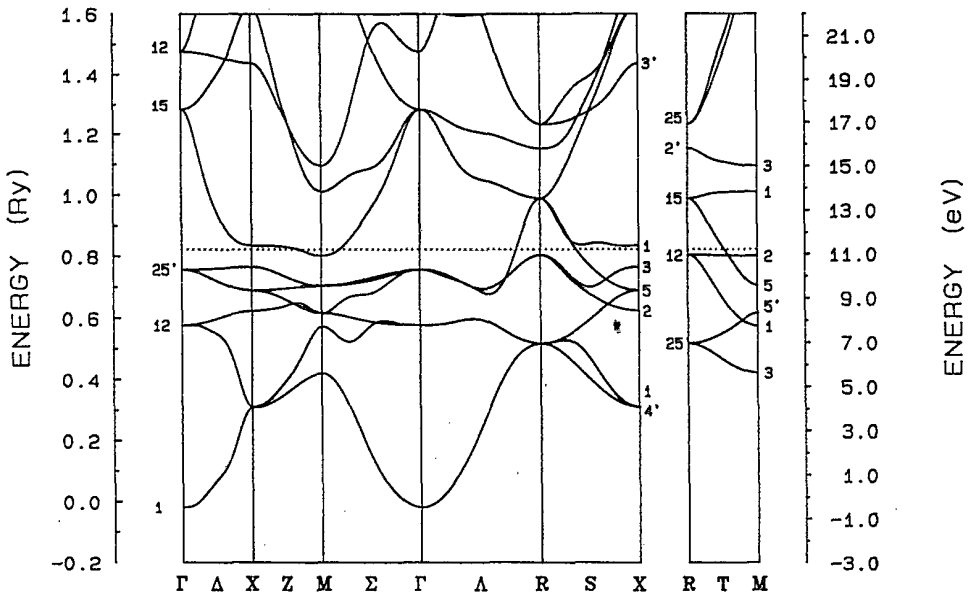

FIG. 7. The band structure along high-symmetry directions of the $B2$ phase of CoAl at the lattice constant $a = 2.862$ Å, calculated by the APW method. The Fermi energy is denoted by the dotted horizontal line.

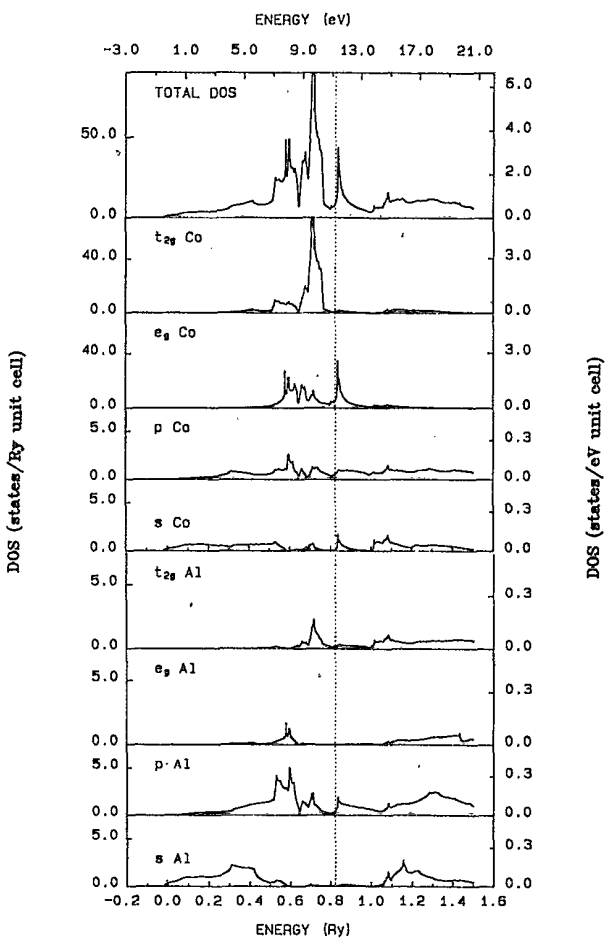

FIG. 8. The density of states of the $B2$ phase of CoAl at the lattice constant $a = 2.862$ Å, as found by the APW method. The top plot shows the total density of states, while the lower graphs show the symmetry-decomposed partial density of states on each atom. The dotted vertical line represents the Fermi energy. Note the different scales between the d and the s,p components of the DOS.

shows the DOS decomposed into the l components on each site. We note the following features: (a) the d Sb states appear mainly above E_F; (b) a strong p Sb component below E_F; (c) a strong s Sb contribution far below E_F; (d) a strong component of d Y states with t_{2g} symmetry above E_F; (e) a pronounced peak of d Y states with e_g symmetry below E_F that strongly hybridize with the p Sb states; and (f) the low DOS at E_F. The Fermi energy, the total DOS, and the decomposed DOS values at the Fermi energy are given in Table VII.

In Fig. 7 the energy bands of $B2$ (CsCl) CoAl are displayed along several symmetry directions. Flat bands occur just above E_F in the XM and RX directions, while another flat band appears below E_F in the RM direction. This suggests that E_F may fall into a DOS minimum between two pronounced peaks. This is confirmed by looking at Fig. 8, which shows the DOS and its various components. We note the following: (a) a strong t_{2g} Co component below E_F; (b) a uniform distribution of the e_g Co DOS with a pronounced peak just above E_F; (c) a small p Al contribution across the entire energy range; and (d) the intriguing possibility that in a Co-rich alloy E_F might fall on a DOS maximum, which could change the electronic properties of this system. The numerical values of E_F and the DOS and l-decomposed DOS are listed in Table VII. We should mention here that this calculation is in agreement with a previous calculation of Nagel[24] in which x-ray spectra were also calculated.

The energy bands of $B2$ RuZr are presented in Fig. 9. The RuZr band structure is very different than that of CoAl, the main characteristic being the narrowness of the d Zr bands that appear below E_F. This feature is also shown in Fig. 10, where the RuZr DOS and its components are presented. Note the very high DOS with t_{2g} and e_g Zr symmetry below E_F and the very low DOS at E_F. Table VII lists E_F, the DOS at E_F, and the l components of the DOS at E_F.

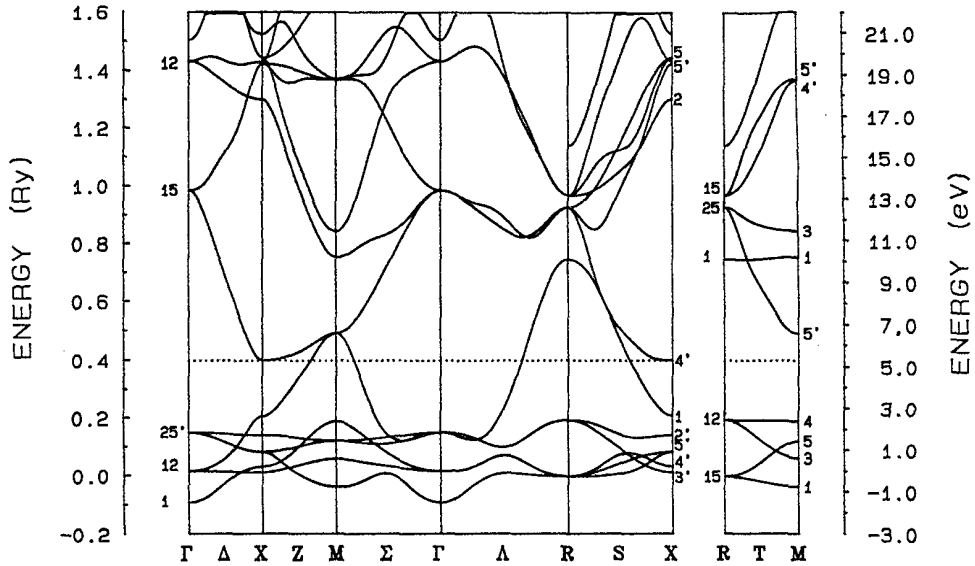

FIG. 9. The band structure along the high-symmetry directions of the $B2$ phase of RuZr at the lattice constant $a = 3.22$ Å, using the APW method to do the calculations. The dashed horizontal line shows the location of the Fermi level.

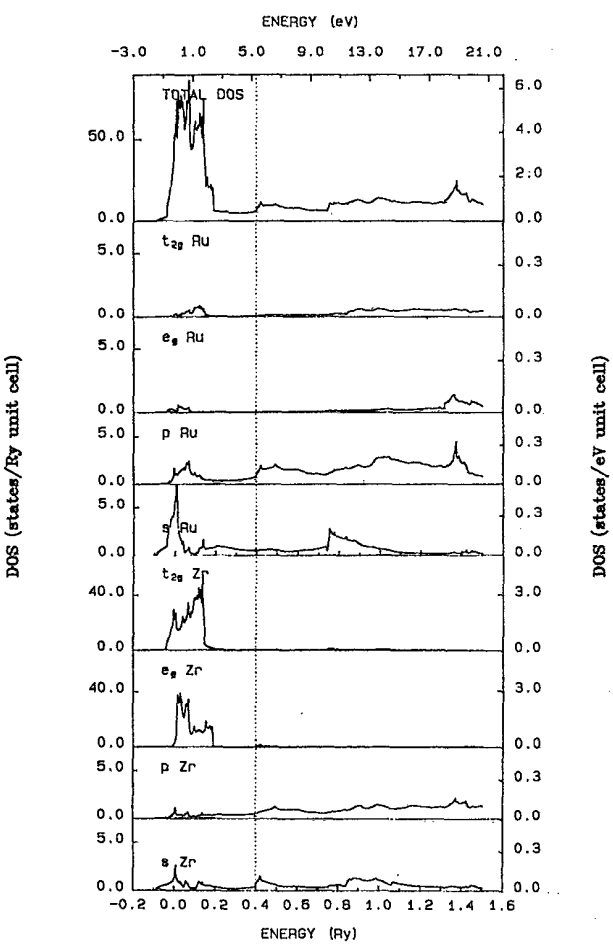

FIG. 10. The density of states of the $B2$ phase of RuZr at the lattice constant $a = 3.22$ Å, calculated via the APW method. The top graph shows the total density of states, while the lower graphs show the symmetry-decomposed partial density of states on each site. The Fermi energy is marked by the dotted vertical line. Note the different scales in the various components of the DOS.

The energy bands and DOS of NbIr in the $L1_0$ structure were calculated using eigenvalues found by the LAPW program at the LDA equilibrium values of the volume and c/a. The energy bands are shown in Fig. 11. The density of states and the l decomposition are shown in Fig. 12. Since our LAPW DOS program[25] is not symmetrized, we cannot distinguish the e_g and t_{2g} d states. Note that although the d Ir states dominate below E_F, the levels near the E_F are composed of nearly equal amounts of d Ir and d Nb states. Table VII lists the DOS and partial DOS at the Fermi energy.

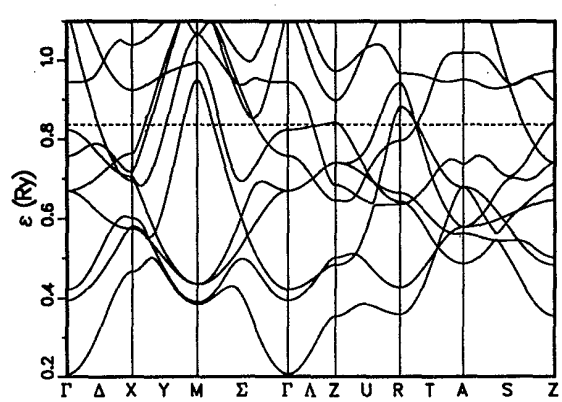

FIG. 11. The band structure along the high-symmetry directions of NbIr in the $L1_0$ phase, as calculated by the LAPW method. The calculation was made at the lattice constants $a = 3.99$ Å using $c = 3.86$ Å using the lattice defined by the primitive vectors (3) and the basis vectors (4). The dotted horizontal line is at the Fermi level.

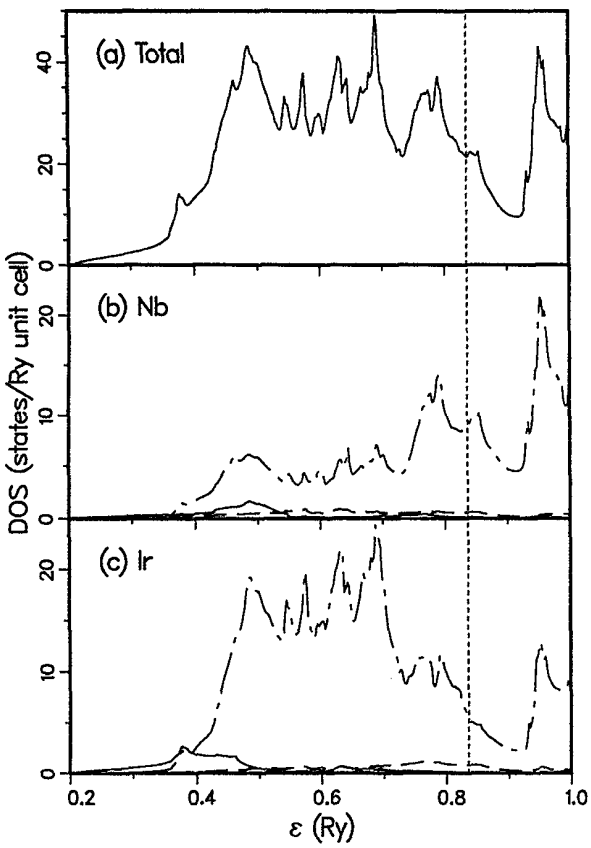

FIG. 12. The density of states of the $L1_0$ phase of NbIr, derived from *ab initio* eigenvectors calculated by the LAPW program using the method developed by Wang.[25] The lattice constants are the same as in Fig. 11. The top graph shows the total density of states. The lower graphs show the l-decomposed partial density of states within each muffin-tin. The solid lines represent the contributions from the *s* partial waves, the dashed lines the *p* partial waves, and the dash-dotted lines the *d* partial waves. The dotted horizontal line is at the Fermi energy.

VI. CONCLUSIONS

We used the LAPW method to perform a set of first-principles, self-consistent, total-energy calculations to determine the equations of state and the elastic constants of SbY in the $B1$ (rocksalt) phase, CoAl and RuZr in the $B2$ (cesium chloride) phase, and NbIr in the $L1_0$ phase. The lattice constants and bulk moduli we determine are in excellent agreement with the available experimental data. We then calculated the strain energies in each crystal to determine the remaining elastic moduli. The numerical uncertainty in this procedure (basically due to the limited basis size and k-point mesh, and to errors in the energy-versus-strain fit) is less than 5% for the cubic materials and 10% for NbIr. Direct measurements of the single-crystal elastic moduli for these intermetallic alloys are not available, but we were able to use our computed C_{ij} to determine bounds on the polycrystalline shear modulus G. The experimental values of G in SbY and CoAl are within our theoretical bounds, so we conclude that our predicted elastic moduli are in good agreement with experiment. In fact, the data for CoAl were provided to us after we submitted this paper.[21] For NbIr the experimentally determined shear modulus is below our calculated lower limit, so the agreement there is not quite as good. This may be due to the fact that the experimental NbIr sample was not stoichiometric. We did not find experimental shear moduli for RuZr, nor did we find any single-crystal measurements of the elastic moduli.

We have also used our calculated elastic moduli and the correlations discovered by Fine *et al.*[1] to predict melting temperatures of the intermetallic alloys. Except for SbY, where the correlation obviously fails, our predicted melting temperatures are all within two standard deviations of the correlations of Fine *et al.*

ACKNOWLEDGMENTS

We are particularly grateful to Dr. R. L. Fleischer for providing us with his data for CoAl (Ref. 21). We also wish to thank S. R. Chubb, D. Singh, H. Krakauer, and K. Sadananda for useful conversations. This work was partially supported by the Office of Naval Research (ONR), U.S. Department of Defense. One of us (J.E.O.) gratefully acknowledges partial support by the Office of Naval Technology. The National Science Foundation provided computer time for part of this work.

[1]M. E. Fine, L. D. Brown, and H. L. Marcus, Scr. Metall. **18**, 951 (1984).
[2]J. Eridon, Philos. Mag. Lett. **59**, 31 (1989).
[3]O. K. Anderson, Phys. Rev. B **12**, 3060 (1975).
[4]S.-H. Wei and H. Krakauer, Phys. Rev. Lett. **55**, 1200 (1985).
[5]S. R. Chubb, D. A. Papaconstantopoulos, and B. M. Klein, Phys. Rev. B **38**, 12 120 (1988).
[6]D. D. Koelling and B. N. Harmon, J. Phys. C **10**, 2041 (1975).
[7]H. J. Monkhorst and J. D. Pack, Phys. Rev. B **13**, 5188 (1976).
[8]L. Hedin and B. I. Lundqvist, J. Phys. C **4**, 2064 (1971).
[9]W. Kohn and L. J. Sham, Phys. Rev. **140**, A1133 (1965); P. Hohenberg and W. Kohn, *ibid.* **136**, B864 (1964).
[10]F. Birch, J. Geophys. Res. **83**, 1257 (1978).
[11]J. F. Nye, *Physical Properties of Crystals* (Clarendon, Oxford, 1985), pp. 146 and 147.
[12]C. Kittel, *Introduction to Solid State Physics*, 4th ed. (Wiley, New York, 1971), Chap. 4.
[13]J. Chen, L. L. Boyer, H. Krakauer, and M. J. Mehl, Phys. Rev. B **37**, 3295 (1988).
[14]E. Schreiber, O. L. Anderson, and N. Soga, *Elastic Constants and Their Measurement* (McGraw-Hill, New York, 1973), pp. 29–31.

[15]W. Voigt, *Lehrbuch der Kristallphysik* (Teubner, Leipzig, 1928).
[16]A. Reuss, Z. Angew. Math. Mech. **9**, 49 (1929).
[17]R. P. Elliott, *Constitution of Binary Alloys, First Supplement* (McGraw-Hill, New York, 1965).
[18]N. Ridley, J. Inst. Met. **94**, 255 (1966).
[19]W. B. Pearson, *A Handbook of Lattice Spacings and Structures of Metals and Alloys* (Pergamon, Oxford, 1967), Vol. 2.
[20]R. L. Fleischer, R. S. Gilmore, and R. J. Zabala, General Electric Materials Research Laboratory Report No. 88CRD310, 1988 (unpublished).
[21]R. L. Fleischer (private communication).
[22]R. L. Fleischer, J. Mater. Sci. **22**, 2281 (1987).
[23]L. L. Boyer, Phys. Rev. B **19**, 2824 (1979).
[24]D. J. Nagel, Ph.D. thesis, University of Maryland, 1977.
[25]C. S. Wang (unpublished).